Compact steam bottoming cycles: model validation with plant data and evaluation of control strategies for fast load changes

Lars O. Nord[a,*], Rubén M. Montañés[a]

[a]*Department of Energy and Process Engineering, Norwegian University of Science and Technology – NTNU, Trondheim, Norway*

Abstract

Power plants installed on offshore oil and gas installations need to be operated in a flexible manner in order to accommodate the variability in heat and power demands. The present paper describes steady-state process model validation based on data from an actual offshore oil and gas installation, dynamic model validation, and evaluation of control strategies for fast load changes. The offshore process configuration consisted of two gas turbines with a once-through heat recovery steam generator located downstream of each gas turbine. One steam turbine received the combined steam mass flow from the two steam generators. The validation data, focusing on the steam bottoming cycle, consisted of one year of operation. Subsequently, a dynamic process model based on a simplified process layout was developed in the open physical modeling language Modelica and validated with reference steady-state and transient software data. The results from the evaluation of control strategies showed the benefits in utilizing feedforward control for the operation of the heat recovery steam generator under fast load changes, and the effectiveness of attemperation to avoid excessive excursions of live steam temperature during transients.

Keywords: model validation, process modeling, heat recovery, combined cycle, process control, transient, Modelica

1. Introduction

The offshore industry for oil and gas extraction and processing relies on flexible and secure supply of heat and power to the platform for the daily operations. Gas turbines are normally installed to provide the platform with heat, electricity, and mechanical drive. The utilization of the energy available in the exhaust gas of the gas turbines of the platform can improve the performance of the system [1]. By implementing waste heat recovery units (WHRU) or bottoming cycles, the energy efficiency on the platform can be increased and the associated CO_2 emissions can be reduced. Several studies have evaluated different bottoming cycles for implementation on offshore oil and gas platforms. Pierobon et al. [2] investigate three different technologies

*Corresponding author
Email address: `lars.nord@ntnu.no` (Lars O. Nord)

for waste heat recovery in offshore oil and gas platforms on a specific offshore platform with gas turbines with a rather low exhaust temperature. The analyzed technologies include steam bottoming cycle, air bottoming cycle, and organic Rankine cycle (ORC), concluding that ORC is the most promising technology long term to best utilize the exhaust energy in the case study, however, steam bottoming cycles were also considered a suitable technology. Another promising technology for implementation offshore is CO_2 bottoming cycles with the potential to increase the net plant efficiency with 10–11%-points compared to a simple cycle gas turbine [3]. Other studies have considered hybrid systems with electrification from land combined with gas turbines [4]. All the analyzed technologies and cycles in the literature have their pros and cons. ORCs have a disadvantage at high temperatures (above 400 °C) due to working fluid degradation; steam cycles need water treatment that can be bulky for an offshore installation; electrification has a disadvantage for providing heat; CO_2 cycles are still immature. Because of the maturity of the technology, the ease in supplying heat from steam extractions, the possibility to recover heat from high-temperature sources, and recent advances in making the components lighter and more compact [5], steam cycles are still considered as one of the most attractive technologies for this application.

Steam bottoming cycles are, as of June 2018, operating on three Norwegian offshore oil and gas installations, as the only bottoming cycles in operation on the Norwegian continental shelf. One of the installations is the Oseberg Field Center where the drum-based heat recovery steam generators (HRSGs), originally installed in 1999–2000, were replaced by once-through heat recovery steam generators (OTSGs) in 2011–2012 for increased compactness and reliability. In general, the offshore steam bottoming cycles have had reliability issues, mostly related to the HRSG. Design considerations for offshore compact steam bottoming cycles are discussed in [6], showing the importance of weight, volume footprint and flexibility as design criteria. Different plant layouts and operating scenarios at both design and steady-state off-design conditions are analyzed in [7] and [8]. Single-objective optimization of the weight-to-power ratio and multi-objective optimization of weight and power are performed in [5] to arrive at low weight and high power solutions. Riboldi and Nord [9] evaluated the effectiveness of combined cycles in offshore oil and gas installations for cogeneration of heat and power exemplifying the attractiveness to do so. A knowledge gap in the literature for these cycles and applications is related to dynamics and flexibility. Pierobon et al. [10] present a methodology to discard optimal process designs based on dynamic requirements by means of dynamic simulations, applied to ORCs in offshore oil and gas installations. Benato et al. [11] study the dynamics of an air bottoming cycle applied to offshore applications. The use of feedforward control for compact OTSGs is mentioned by Brady [12], but only qualitatively. For dynamic studies on control strategies for compact steam bottoming cycles, no work is available in the open literature to the authors' knowledge.

For combined gas and steam turbine cycles, and steam bottoming cycles, several works related to dynamics are available in the literature. This includes model validation [13], part load operation [14], startup [15], system response to step disturbances [16], as well as steam cycle component design [17] and dynamics

[18, 19]. However, the cited works consider non-compact designs. Compact steam bottoming cycles, preferably with low footprint and weight, have special considerations related to material selection, process layout, and component design, all of which effect the system dynamics.

On offshore oil and gas installations, the power demand is high and changes over time both in day-to-day operation and over the lifetime of the installation. The power plant should be flexible to always be able to adjust to the needs of the oil and gas processes on the platform while being compact with low weight. Key aspects of operational flexibility include part load efficiency and emissions, and the transient performance under load changes. A validated dynamic process model can help to develop understanding on the transient performance of the system, and to evaluate control strategies and the feasibility of operation of new process designs at the design stage. The novelty of this work are the analyses of the dynamic performance of a compact steam bottoming cycle designed for offshore installations, and the development of a control strategy, using model based control design, to operate under fast load changes for such a cycle. This is moving one step forward from previous study related to steady-state off-design operation for compact steam bottoming cycles [7]. Although the case study in this paper was applied to an offshore installation, a compact steam cycle can also be attractive on ships and other locations with space and weight constraints. This expands on the applications for this work. Another valued aspect of the paper is the model validation with industrial plant data from an actual compact steam bottoming cycle. This type of information is scarce in the literature. Therefore, the primary objectives of this paper were:

- Development and validation of a steady-state process model with industrial plant data from a compact steam bottoming cycle at the Oseberg Field Center.
- Development and validation of a dynamic process model with focus on steam cycle transient performance.
- Evaluation of a case study on decentralized control structures for fast load changes in compact steam bottoming cycle.

2. Methodology

In order to achieve the objectives of this work, the following methodology was developed, as summarized in Fig. 1. A steady-state model of the offshore combined cycle power plant was developed, as described in Section 2.1 (2 GTs + 2 OTSGs + 1 ST). The steady-state model was validated with plant data from the Oseberg Field Center for close-to-design point and off-design steady-state operating conditions. The Thermoflow software suite was used to develop a design of a process layout of a combined cycle plant with similar geometry and process conditions as the Oseberg plant [20]. The tool outputs detailed data on OTSG and ST sizing, as well as reference data for dynamic process model validation under steady-state off-design

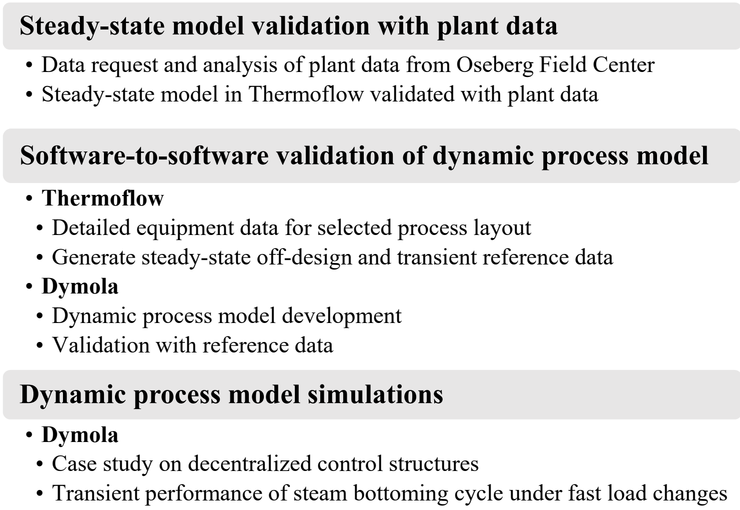

Figure 1: Methodology used for process model validation.

and transient operating conditions driven by GT load changes. Subsequently, a dynamic process model of a simplifed layout was developed in the Modelica language [21], as described in Section 2.2 (1 GT + 1 OTSG + 1 ST). Modelica is a physical modeling language, which has been utilized in the literature for the development of dynamic process models of thermal power plants onshore [22, 23, 24, 25]. A software-to-software validation method was employed for the validation of the dynamic process model with the reference steady-state and transient data. Finally, the dynamic process model was employed to test different algorithms and control strategies of the steam cycle to handle fast load changes driven by GT load change.

2.1. Process and steady-state model description

The combined cycle on the Oseberg Field Center, located in the North Sea, consists of two GE LM2500+ gas turbines that each drives an export gas compressor. Downstream of each GT is a once-through heat recovery steam generator. The GTs and OTSGs are located on the Oseberg D platform, whereas the ST, which is connected to an electric generator, is located on the Oseberg A platform. Since the OTSGs and the ST are located on different platforms, there is a long steam supply pipe of about 400 m connecting them. The two OTSGs are designed for a live steam pressure of 16.5 bar(a) with a live steam temperature of 430°C and a total steam mass flow rate of 17.5 kg/s.

The process flow sheet of the Oseberg model is shown in Fig. 2, and model assumptions are listed in Table 1. In addition, detailed Oseberg plant data on OTSG geometry, including sections, tubing and fin geometry were included as inputs. The process design, modeling, and simulation tool Thermoflow version 25.0 was used [20]. For the water and steam properties, the IAPWS-IF97 formulation was used [26]. Gas-side heat transfer convective correlations were based on ESCOA® [27].

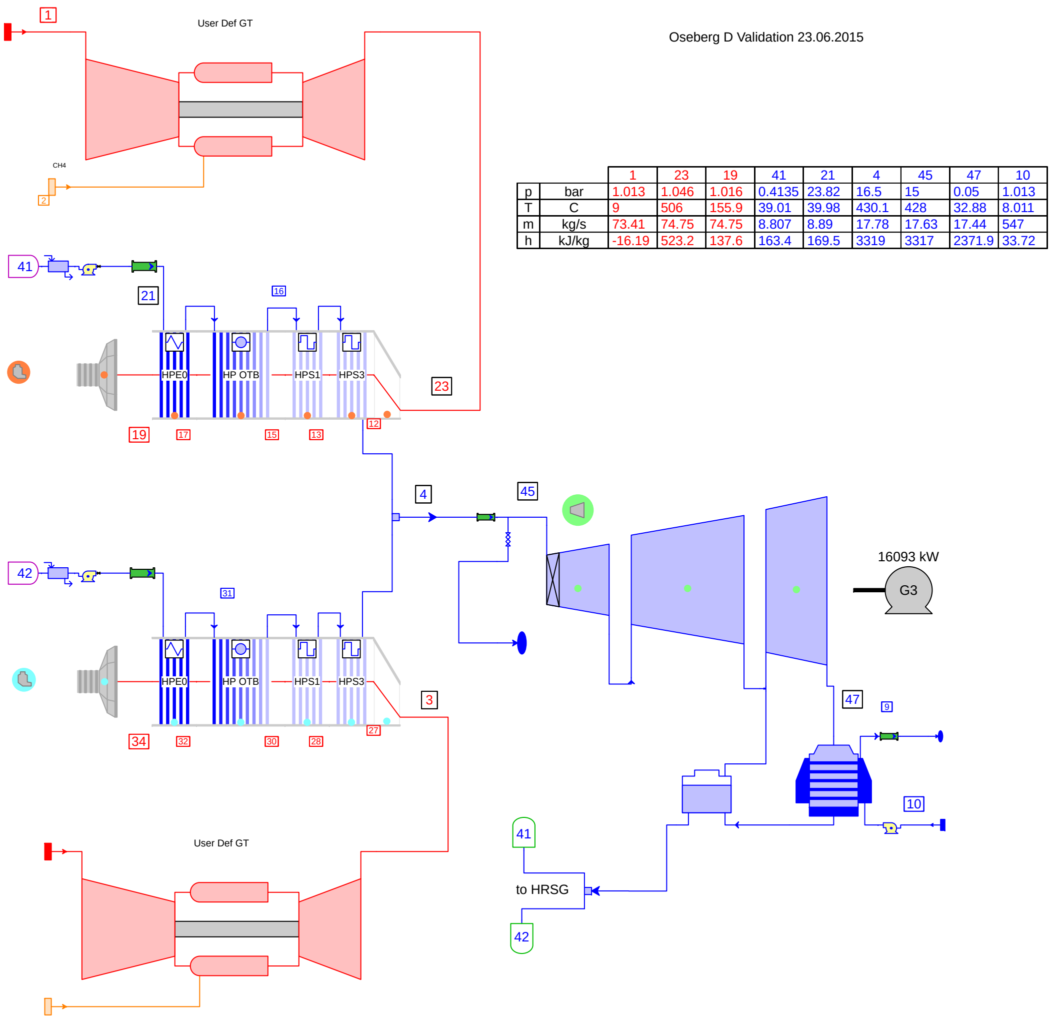

		1	23	19	41	21	4	45	47	10
p	bar	1.013	1.046	1.016	0.4135	23.82	16.5	15	0.05	1.013
T	C	9	506	155.9	39.01	39.98	430.1	428	32.88	8.011
m	kg/s	73.41	74.75	74.75	8.807	8.89	17.78	17.63	17.44	547
h	kJ/kg	-16.19	523.2	137.6	163.4	169.5	3319	3317	2371.9	33.72

Figure 2: Thermoflow process model of the combined cycle gas turbine plant located on the Oseberg A and D offshore oil and gas platforms. Selected stream data close-to-design point are included. The model was validated with plant data from 23 June 2015.

Table 1: Process model assumptions.

Site	
Ambient T (°C)	9
Ambient pressure (bar)	1.013
Ambient relative humidity (%)	60
Frequency (Hz)	60
Cooling water system	Direct water cooling
Cooling water	Sea water
Cooling water T (°C)	8
Gas turbine	
GT fuel	Methane
Lower heating value (kJ/kg)	50047
OTSG	
Tube material	Incoloy
Fin material	TP 409
Fin type	Serrated
Tube layout	Staggered
Steam turbine	
Control mode	Sliding pressure / throttle control
Rotational speed (rpm)	3600

The steam turbine efficiency was calculated by the method explained in Spencer et al. [28]. The efficiency of each step within a particular steam turbine section was considered the same in the absence of steam moisture. This efficiency is defined as the dry step efficiency. To correct for condensing moisture entrained with the steam, the efficiency of a step with wet steam is reduced in proportion to the average moisture present within that step. The Wilson line represents the steam equilibrium quality at the onset of condensation within the steam turbine. Because of the high velocity and rapid cooling of the steam, it becomes supersaturated before liquid droplets actually begin to form. The selected definition of the Wilson line is that it corresponds to an equilibrium quality of 0.97. All steps whose exit quality is below the Wilson line have their efficiency corrected as follows:

$$\eta_{step} = \eta_{dry} - \beta \left(1 - x_m\right) \tag{1}$$

where η_{step} is the corrected step efficiency, η_{dry} the dry step efficiency, x_m the mean step steam quality, and β the Baumann coefficient. The Baumann coefficient was set to 0.72.

Dry exhaust loss is a function of the annulus velocity in the steam turbine exhaust. Further, the exhaust loss was corrected for wetness according to [28]:

$$w_{st,loss} = w_{dry,loss} \cdot 0.87(1 - y)(1 - 0.65y) \tag{2}$$

where $w_{st,loss}$ (kJ/kg) is the exhaust losses corrected for wetness, $w_{dry,loss}$ the dry exhaust losses, and y the moisture content $(1 - x)$.

2.2. Dynamic process model

A Dynamic process model of the combined cycle were developed with Modelica, by means of the modeling and simulation environment Dymola [29]. The Modelica Thermal Power Library (TPL) was utilized for dynamic process modeling [30]. The library contains the main process submodels of the plant including recuperators in OTSG (economizer, evaporator, and superheater sections), steam expansion sections in steam turbine, condenser, pumps, valves, flow resistances, and regulation elements (PID, multipliers, ramps). The process models were modified, parameterized and combined to develop the process model of the combined cycle power plant process layout described in Section 2.2.1. The main purposes of application of the dynamic process models were transient performance estimation and development of decentralized control strategies during online plant operation. Therefore, the models were developed to capture the key system level physical phenomena that occur during transient load change of a combined cycle power plant driven by GT load changes. The focus was on OTSG and steam cycle transient performance.

2.2.1. Process layout

For dynamic process simulation, detailed data of the equipment are required. That includes dimensions, materials, and geometries of heat exchangers, and fluid inventories within process equipment. Thermoflow

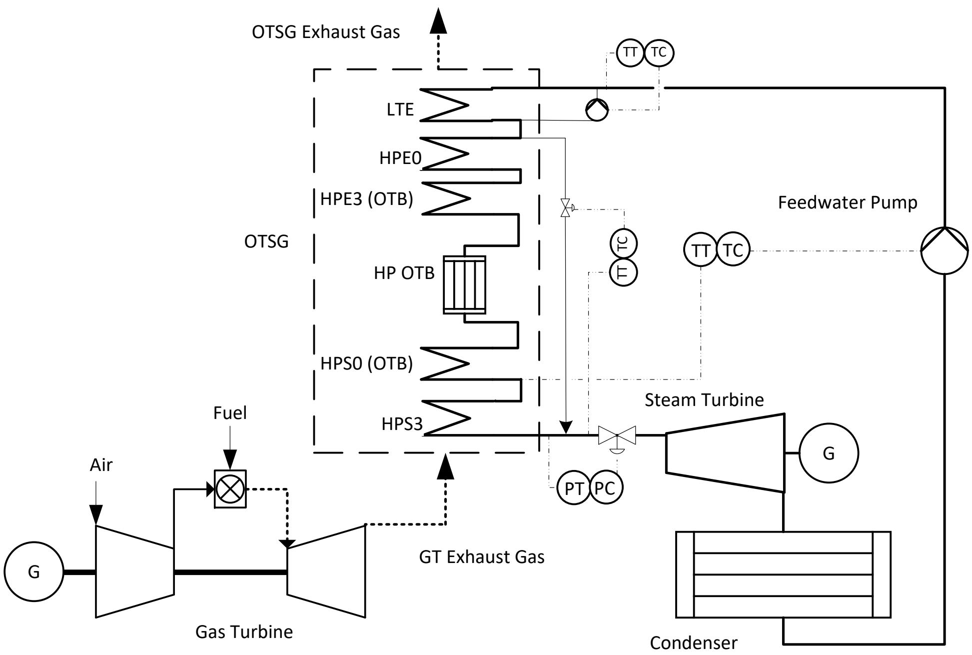

Figure 3: Process layout of the combined cycle power plant. The simplified process layout consist of a 1 GT + 1 OTSG + 1 ST configuration. The OTSG has six recuperators consisting of low temperature economizer (LTE), economizers (HPE0 and HPE3), once-through boiler (HP OTB), and superheaters (HPS0(OTB) and HPS3). The main transmitters and controllers are shown (TT=temperature transmitter; TC=temperature controller; PT=pressure transmitter; PC=pressure controller).

was utilized to obtain a design of the components to be used for dynamic process simulation purposes. The layout consisted of a 1 GT + 1 OTSG + 1 ST configuration, refer to Fig. 3. The reasons for the different layout and steam data compared to the actual Oseberg plant were two-fold:

1. One of the objectives with the dynamic modeling was to perform software-to-software validation. The Thermoflow software only allows for dynamic simulations for simple layouts.
2. The steam data (pressures, temperatures) in Oseberg are based on the original design from the 90s. For this work on control strategies, it was more applicable to use close-to-optimium values based on recent academic work rather than the conservative values from the actual plant [5, 6, 7].

The model of the exhaust gas from the gas turbine consists of a mixture of Ar, H_2O, O_2, N_2 and CO_2. The exhaust gas, at near atmospheric pressure, was modeled with ideal gas thermodynamic equation of state and the thermochemical properties were calculated based on a seven coefficient version of NASA ideal gas properties. The thermophysical property package based on the IAPWS-IF97 standard with analytical derivatives was used for the water/steam fluid [26]. The media property packages were obtained from the TPL [30].

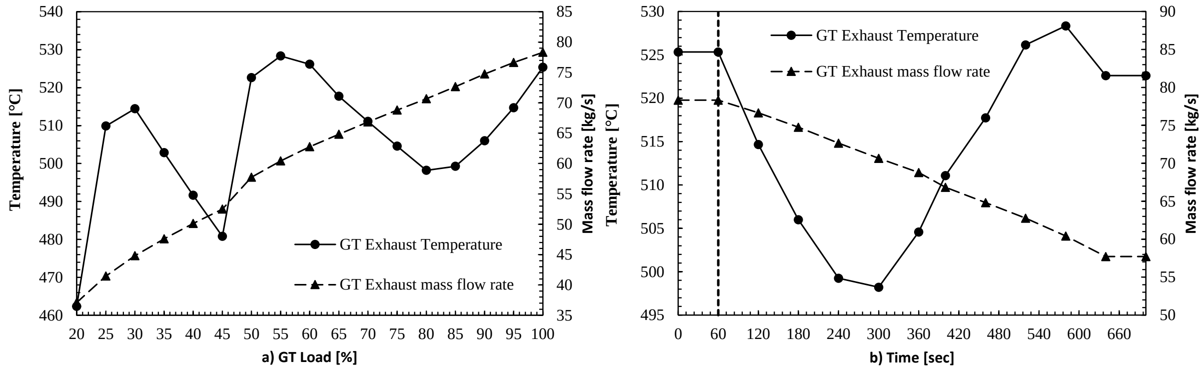

Figure 4: GT exhaust mass flow rate and temperature for off-design loads. a) Steady-state results from simulations of the GE LM2500+ gas turbine for 17 different off-design loads from 100% to 20% GT Load. b) Tailormade time dependent trajectory: boundary conditions and disturbance to the steam cycle dynamic process model for a load change from 100% to 50% GT load. The transient event is driven by GT load reduction with a 5%/min ramp rate.

2.2.2. Gas turbine

Dynamic process simulations of combined cycle power plants with focus on load change transient performance of the steam cycle was modeled by considering the GT as a quasi-static element. With the quasi-static method, the GT system is considered to be in equilibrium at each point in time, thus the transient behavior is a succession of off-design results. Following a similar modeling methodology as by Dechamps [31], the GT exhaust temperature and mass flow rate were utilized as a boundary condition and disturbance to the dynamic process model of the steam cycle. This methodology of gas turbine modeling was previously presented by Montañés et al. [24]. GT models contained in Thermoflow were utilized to generate the off-design characteristics of the GE LM2500+ gas turbine. These off-design GT models are validated with industrial data by the software developers. Fig. 4a shows 17 equidistant load operating conditions ranging from 100% to 20%, operated with the site specific conditions presented in Table 1. By assuming a ramp rate, the transient GT exhaust characteristics in terms of mass flow rate and temperature can be tailormade. In between simulated equilibrium points, linear interpolation values were utilized, refer to Fig. 4b.

2.2.3. Steam turbine

The steam turbine section models were also quasi-static models. For load change transient estimation of combined cycles during power plant online operation, it is common to disregard the rotor dynamics and thermal inertia phenomena of the steam turbine [22]. The model consisted of a constant dry step isentropic efficiency for all sections, corrected by the Baumann's formula for the condensing section (LP) as described in Section 2.1. For off-design calculations, the flow characteristics was defined by Stodola's law of cones, refer to Eqs. (3) and (4), where K_t is the flow area coefficient, and n, i and o stand for nominal, inlet and outlet, respectively. The generator model was a simplified model in which the power supply was equal to the power demand, meaning that the rotating frequency was constant. A constant generator efficiency of 0.99 was assumed.

$$K_t = \frac{\dot{m}_n}{\sqrt{p_{i,n}\rho_{i,n}(1-(\frac{p_{o,n}}{p_{i,n}})^2)}} \tag{3}$$

$$\dot{m}_t = K_t\sqrt{p_i\rho_i(1-(\frac{p_o}{p_i})^2)} \tag{4}$$

2.2.4. OTSG

A dynamic process model of the OTSG was developed by using generic heat exchanger recuperator models from the TPL [30]. The OTSG was built up from six recuperator models representing the six heat exchangers as shown in Fig. 3. The heat exchanger models were parameterized considering the tubing geometries, size, and materials obtained from the design, which were based on the Oseberg plant heat exchanger geometry, tubing, and fin data, refer to Section 2.2.1. The recuperator model consisted of a model of a shell and tube heat exchanger with a two-phase medium on the secondary (tube) side and gas on the primary (shell) side, and a wall model.

The gas side model consisted of a discretized 1-D pipe model with lumped pressure. Static mass, mass-fraction, and energy balance equations were discretised in n volume segments with the finite volume method. The state variables were one pressure p (lumped), n temperatures, and mass fractions. A convective heat transfer correlation for gas flow over tube bundles was utilized to calculate the heat transfer coefficient for each volume, according to Eq. (5). Here F_a is a tube arrangement factor, λ is the thermal conductivity of the gas and d_{hyd} is the hydraulic diameter of the pipe. The Nusselt number Nu_o for each volume is calculated by Reynolds dependent correlations from [32].

$$\alpha_g = \frac{F_a Nu_o \lambda}{d_{hyd}} \tag{5}$$

A similar modeling approach was considered for the single-phase and two-phase flows on the water/steam side, in which dynamic energy and mass balances were considered. The general mass balance is presented in Eq. (6), where ρ is density, p is pressure and h the specific enthalpy. The general energy balance is shown in Eq. (7). Note that in the model, the energy and mass balances were also discretized in the longitudinal direction of the pipe in n volumes.

$$\frac{dm}{dt} = V\left(\frac{d\rho}{dh}\frac{dh}{dt} + \frac{d\rho}{dp}\frac{dp}{dt}\right) \tag{6}$$

$$V\rho\frac{dh}{dt} = \dot{m}_{in}h_{in} - \dot{m}_{out}h_{out} + V\frac{dp}{dt} + Q \tag{7}$$

The radial heat transfer was calculated with Eq. (9). For the steam/water side, a heat transfer correlation was used for estimating convective heat transfer coefficient for superheaters, α_s, for single-phase flow, described in Eq. (8). A similar formulation was employed for the economizer. The mean Nusselt number, Nu_m, was calculated by Reynolds number dependent correlations from [32].

$$\alpha_s = \frac{Nu_m \lambda}{d_{hyd}} \tag{8}$$

$$Q = \alpha_s A_{heat} \left(T_{wall} - T_{fluid}\right) \tag{9}$$

For the two-phase flow in the boiler section, a constant heat transfer coefficient for the cold side was implemented with a value of 21 kW/m^{2}K [33]. This is a common modeling assumption for two-phase flow in system level simulations, in which the boiling process is reduced to the saturated boiling regime [34]. An alternative approach is to use a modified Dittus-Boelter equation for the heat transfer coefficient of the liquid. This is then multiplied by an enhancement factor that depends on the steam quality and the Boiling number, as utilized by Benato et al. [22]. The solid wall model was employed for considering transient conductive heat transfer where the heat capacity was lumped at the center of the wall.

2.2.5. Condenser

A surface cooled condenser model with two-phase equilibrium was obtained from the TPL. It consisted of a model of a cylindrical condenser where thermodynamic equilibrium is assumed between the liquid and vapor phase. A dynamic wall model separated the cooling water (tube side) from the water/steam (shell side). A heat transfer correlation for film condensation over tube bundles was used for the shell side heat transfer [32]. The condenser model included a hotwell model where liquid water accumulates. The condenser process model was parameterized with the steady-state simulation output data.

2.3. Control strategies

A common method for operation of the OTSG for off-design GT loads is in sliding pressure mode. The control structure normally consists of a main control loop that manipulates the feedwater mass flow rate to control the live steam temperature [12]. Another option was evaluated in our study: the steam temperature at the outlet of the boiling section of the OTSG (section HPS0(OTB) in Fig. 3) was controlled to set value. This ensured having only dry steam at the superheating section at off-design GT loads; refer to control structure A in Table 2. As shown in Fig. 3, the feedwater pump controller manipulated the variable speed pump (time constant of 5 s) to control the steam temperature at the outlet of heat exchanger HPS0(OTB). In addition, a control loop for feedwater temperature control was included, in which water from the LTE outlet was recirculated to the LTE inlet to ensure that the temperature was above 60 °C for low temperature corrosion control. Attemperation was implemented to limit the live steam temperature to the maximum value of 450 °C, by injecting HP water from the LTE outlet. Finally, a live steam pressure control loop was included. This controller was active at low power plant operation loads (from live steam pressure of 18.75 bar). This corresponded to GT loads of around 50% at site ambient design conditions. This means, that down to 18.75 bar the OTSG was operated in sliding pressure, but at lower loads the control structure was switched towards a throttle control strategy.

The control structures studied are presented in Table 2. For all control structures, the feedwater mass flow rate was manipulated to control either the temperature of the steam at the outlet of the boiler section of the OTSG, $T_{HPSOs,out}$, (control structures A and B) or the live steam temperature (control structures C, D, and E). Both feedforward and feedback control algorithms were tested. In a feedback control scheme, the error signal between set value and measured value is used as an input to the controller. On the other hand, in a feedforward control scheme, the controller respond once the disturbance is applied. It is designed based on process knowledge or a mathematical model, without having to wait for an error in the controlled variable to occur [35]. For control structures A and B, the attemperation controller was active, and they differ in the controller algorithm implemented in the mass flow rate control loop, being feedforward (FF) in control structure A and feedback (PI) in control structure B. Control structure C implemented feedback control (PI) on the feedwater mass flow rate control loop while control structure D implemented feedforward control. Both control structures C and D had the attemperation controller deactivated. Finally, in control structure E, attemperation was activated for tight control of live steam temperature during the transient event with a parallel feedforward and PI controller on the main control loop. The control structures were evaluated under two load changing scenarios:

- Scenario 1: deloading from 100% to 50% GT load with a ramp rate of 10%/min
- Scenario 2: loading from 50% to 100% GT load with a ramp rate of 10%/min

3. Results and discussion

3.1. Steady-state process model results

Steam turbine generator active power for a full year is shown in Fig. 5. Two areas, indicated by boxes, were considered interesting for operation close to the design point (leftmost box) and for a steam turbine part load point (rightmost box). The active power was plotted to ensure that the selected data sets were based on steady operation over a longer period, however, the specific selection of data sets within the highlighted areas was based on live steam pressure and feedwater mass flow rate.

Based on a close-to-design point, process configuration and stream data are shown in Fig. 2. A comparison between plant data and simulation results are shown in Table 3. Compared to plant data, the difference in

Table 2: Control structures for the steam bottoming cycle. The feedwater mass flow rate was utilized to control the live steam temperature $T_{livesteam}$ or the temperature of the water/steam at the outlet of the HPS0 superheater $T_{HPSOs,out}$. The control loop included a feedback controller (PI) or a feedforward controller (FF). For three of the control structures, the live steam attemperation control loop was active.

Control Structure	**Controlled variable**	**Controller**	**Attemperation**
A	$T_{HPSO,out}$	FF	Yes
B	$T_{HPSO,out}$	PI	Yes
C	$T_{livesteam}$	PI	No
D	$T_{livesteam}$	FF	No
E	$T_{livesteam}$	FF + PI	Yes

Table 3: Comparison of process simulation results with plant data at OTSG design point.

	Plant data	**Process simulation**
$T_{livesteam}$ (°C)	430	430
$p_{inletHRSGsteam}$ (bar(a))	23.7	23.8
$p_{livesteam}$ (bar(a))	16.6	16.5
$p_{inletST}$ (bar(a))	15.0	15.0
$T_{inletHRSGgas}$ (°C)	507	506
$T_{outletHRSGgas}$ (°C)	156	156
$\dot{m}_{steam}$ (kg/s)	18.2	17.8
$\dot{W}_{ST}$ (MW)	16.1	16.1

generator active power was 0.2% and the difference in steam mass flow rate at OTSG outlet was 2.1%. The gas outlet temperature from the OTSG was close to identical.

The selected operational area for off-design conditions (steam turbine part load), was based on operation of one of the two OTSGs. The live steam pressure was kept close to design but the steam mass flow rate was close to half of the design value. The active power output was 7.9 MW for both plant data and model results. The difference was in the order of 0.1%. Overall, the match between model results and plant data was deemed satisfactory. These results contribute to strengthen the common consideration of Thermoflow's steady-state process models as a reference of state-of-the-art performance of gas turbine based thermal power plants, as has been discussed in previous work in literature [36].

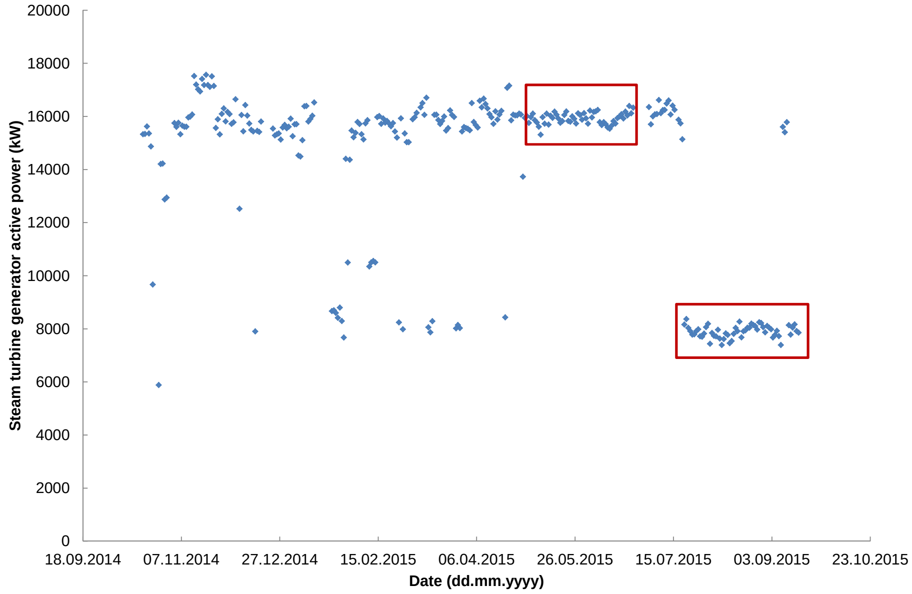

Figure 5: Oseberg A steam turbine generator active power over a year. One data set per day was collected. Boxed regions indicate data of interest to design and off-design model validation respectively.

3.2. Dynamic process model results

3.2.1. Validation of dynamic process model with steady-state data

The dynamic process model of the process layout in Fig. 3 was validated with steady-state reference data. The relative errors (REs) for the considered process variables are presented in Table 4 and calculated with Eq. (10), where t_r is the reference value from the steady-state simulations and t_s is the simulation result in Dymola when the process reaches steady-state conditions.

$$RE = 100\frac{t_s - t_r}{t_r} \tag{10}$$

The predictions of the process model for steam turbine generator active power, live steam temperature, and live steam mass flow rate were close to the reference data. The good prediction of the pressure at steam turbine inlet shows the suitable functioning of the control structure. It was implemented as sliding pressure mode down to 40% GT load, after which the pressure was throttle controlled. This yielded zero RE since the pressure was kept at set point by the valve controller. The results of feed water temperature at economizer outlet ($T_{HPEOs,out}$) and the recirculated water mass flow rate for feedwater ($\dot{m}_{LTE,rec}$) temperature control shows the suitable implementation of the low temperature corrosion controller. The live steam pressure at steam turbine inlet was slightly overpredicted by the process model, for the region at which the OTSG is operated under sliding pressure mode, but the RE was within 1.7%. The steam flow rate was also properly predicted by the dynamic process model, with a deviation within 1.5%. The mean average error for the gas

Table 4: Relative errors, calculated with Eq. (10), of dynamic process simulation results in Dymola with reference data for the process layout described in Section 2.2.1.

	100% GT load	**80% GT load**	**60% GT load**	**40% GT load**	**20% GT load**
$p_{inletST}$	1.54	1.67	1.47	0.00	0.00
$T_{HPS1s,out}$	0.21	0.13	0.32	0.27	0.32
$T_{HPE0s,out}$	1.1	0.72	1.13	0.16	-0.49
$\dot{m}_{LTE,rec}$	2.53	1.49	-2.79	-3.88	3.57
$\dot{m}_{steam}$	1.38	1.40	1.31	1.54	1.49
$\dot{W}_{ST}$	-0.70	-0.83	-1.10	-1.25	0.00

temperature profile within the OTSG was within 0.27% (not shown in table), which means that the heat transfer rate distribution within the different recuperators of the OTSG was properly calculated. These results show the capabilities of the dynamic process model to capture the steady-state performance of the process at close to the design point, and for several steady-state off-design GT loads describing the whole operating window of the process (100% down to 20% GT load). This also shows that the implemented control structure in the model brings the process to stabilization at different operating conditions, and the suitable implementation of the regulatory control layer of the steam cycle.

Results of steady-state off-design performance for the process layout when the GT was operated at different loads are shown in Fig. 6. The results are presented as a percentage of the value of the steam cycle process variable at design conditions, which corresponds with 90% GT load. The results were obtained with the dynamic process model and the results were influenced by the control structure applied in the steam cycle. In this case, feedwater mass flow rate was manipulated to control the steam temperature at the outlet of the boiling section of the OTSG, refer to Section 2.3 and control structure A in Table 2. The results allow to map the off-design performance of the main process variables of the plant at reference ambient conditions.

3.2.2. Validation of dynamic process model with reference transient data

The transient reference data corresponded to the transient performance of the steam cycle during load changes in the GT, consisting of a deloading from 100% GT load to 50% GT load, at time $t = 5$ min, followed by a load increase from 50% to 100% GT load at time $t = 70$ min. The load change ramp rate was 10% GT load/min. The transient response in terms of steam turbine power output and live steam mass flow rate are presented in Fig. 7. The results show that the dynamic process model can properly predict the transient output trajectory of the selected main process variables.

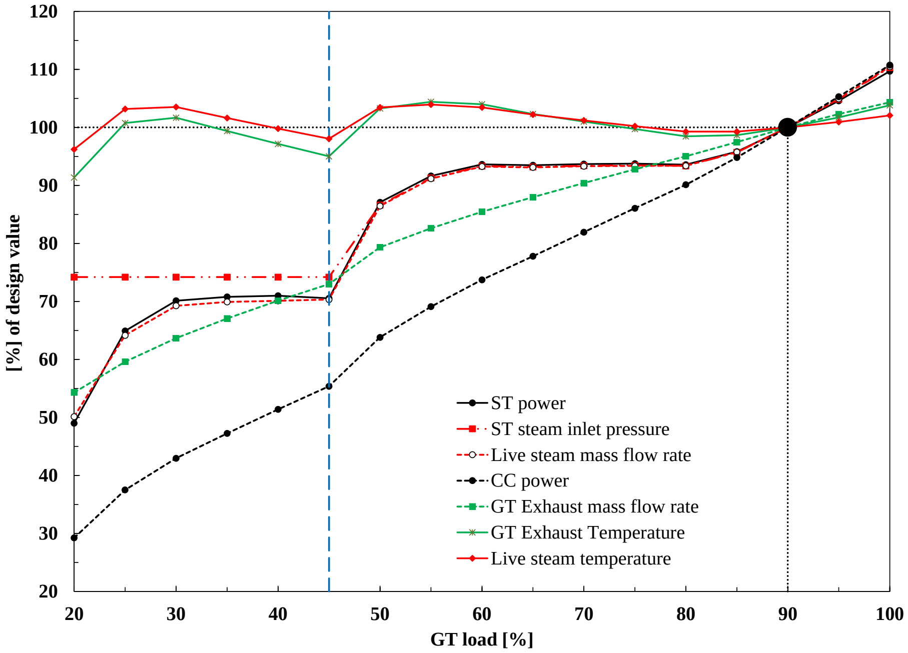

Figure 6: Steady-state results from dynamic simulations for the combined cycle operated at off-design GT loads ranging from 100% to 20%. The steam cycle design point was at 90% GT load. The vertical line separates the sliding pressure operation strategy (high GT loads) from the steam pressure throttle control strategy (low GT loads). Reference values for process variables at design point: ST active power 10.3 MW, ST steam inlet pressure 25.3 bar, live steam mass flow rate 10.5 kg/s, live steam temperature 462.9°C, GT exhaust temperature 505.4 °C, GT exhaust mass flow rate 453.5 kg/s, combined cycle power 35.8 MW.

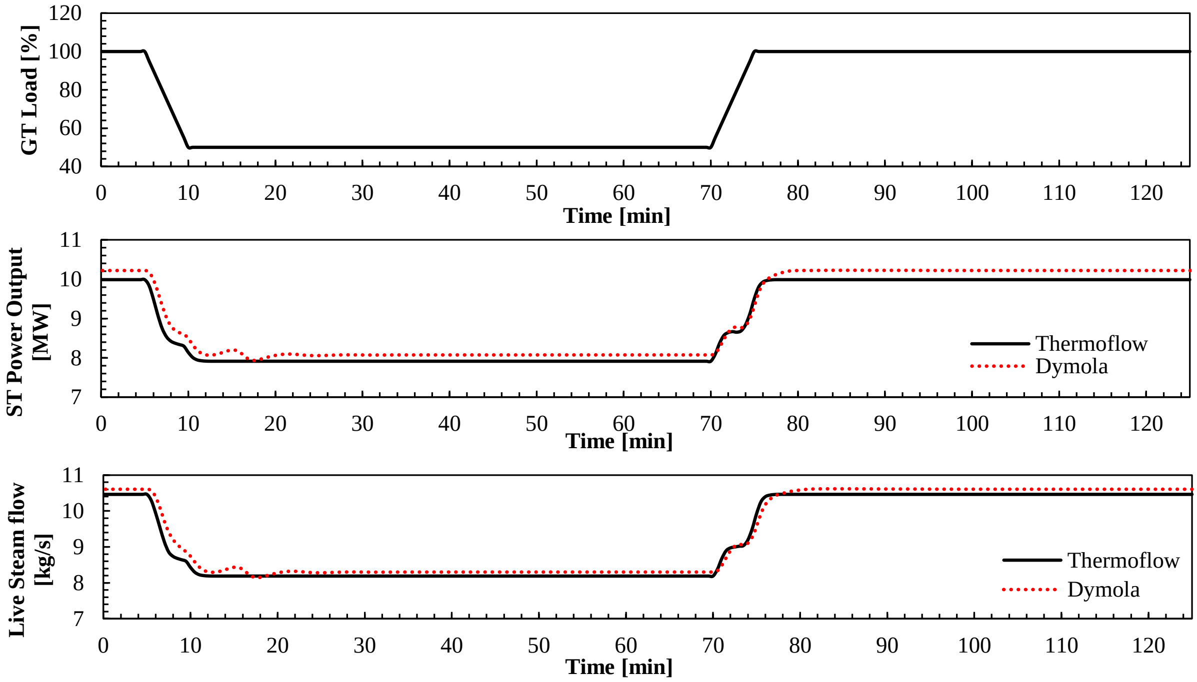

Figure 7: Dynamic process model validation results. Comparison between transient simulation results in Thermoflow and Dymola. Steam turbine active power and live steam flow rate output trajectories for a load change driven by GT load decrease and increase between 100% and 50% GT loads with a ramp rate of 10% GT load/min.

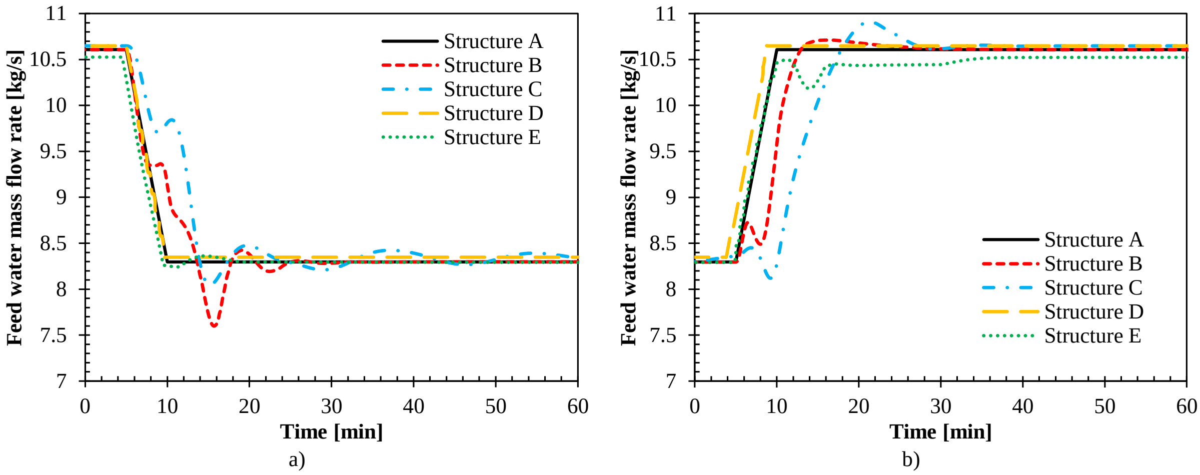

Figure 8: Transient response of the feedwater mass flow rate for a) Scenario 1 and b) Scenario 2.

3.3. Evaluation of decentralized control structures

Dynamic simulations were performed to show the transient performance of the system during load changes when different control structures were applied in the steam cycle, refer to Table 2. The transient response of the main process variables of the steam cycle were studied for two scenarios:

- Scenario 1: Deloading from 100% GT load to 50% GT load, at time $t = 5$ min with a rate of GT load change of 10%/min, refer to Figs. 8, 9, and 11. Fig. 8a shows the feedwater mass flow rate trajectories during the transient event. Fig. 9 shows the transient response of the steam cycle to the load change in Scenario 1. The process variables shown are steam turbine active power (Fig. 9a), live steam temperature (Fig. 9b), live steam pressure (Fig. 9c), and live steam flow rate (Fig. 9d). In addition, the temperature of the water/steam at the outlet of the HPS0 is presented in Fig. 11a. The results are shown for the different control structures defined in Table 2.

- Scenario 2: Load increase from 50% to 100% GT load at time $t = 5$ min with a rate of GT load change of 10%/min; refer to Figs. 8, 10, and 11. Fig. 8b shows the feedwater mass flow rate trajectories during the transient event. Fig. 10 shows the transient response of the steam cycle to the load change in Scenario 2. The process variables shown are steam turbine active power (Fig. 10a), live steam temperature (Fig. 10b), live steam pressure (Fig. 10c) and live steam flow rate (Fig. 10d). In addition, the temperature of the water/steam at the outlet of the HPS0 is presented in Fig. 11b. The results are shown for the different control structures defined in Table 2.

In Scenario 1, when comparing control structures A and B in which $T_{HPSOs,out}$ was controlled by manipulating the feedwater mass flow rate, it is observed that the feedforward controller in Structure A brings the processes towards stabilization faster and with less oscillations around the final steady-state

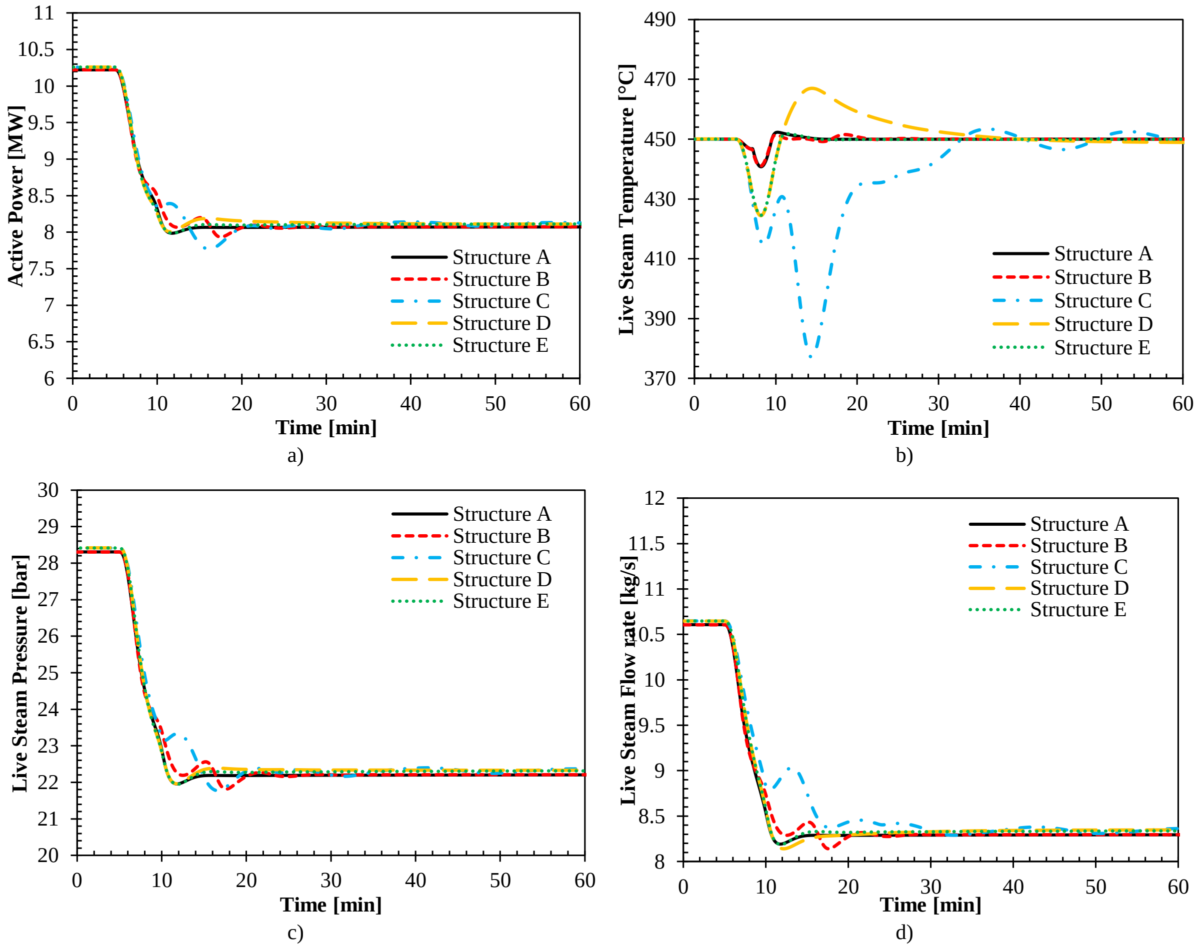

Figure 9: Transient response of the steam cycle to changes in GT load from 100% to 50% with a GT load change ramp rate of 10%/min, starting at time $t = 5$ min (Scenario 1). The response is presented for the five control structures defined in Section 2.3 for: a) steam turbine active power; b) live steam temperature; c) live steam pressure; and d) live steam flow rate.

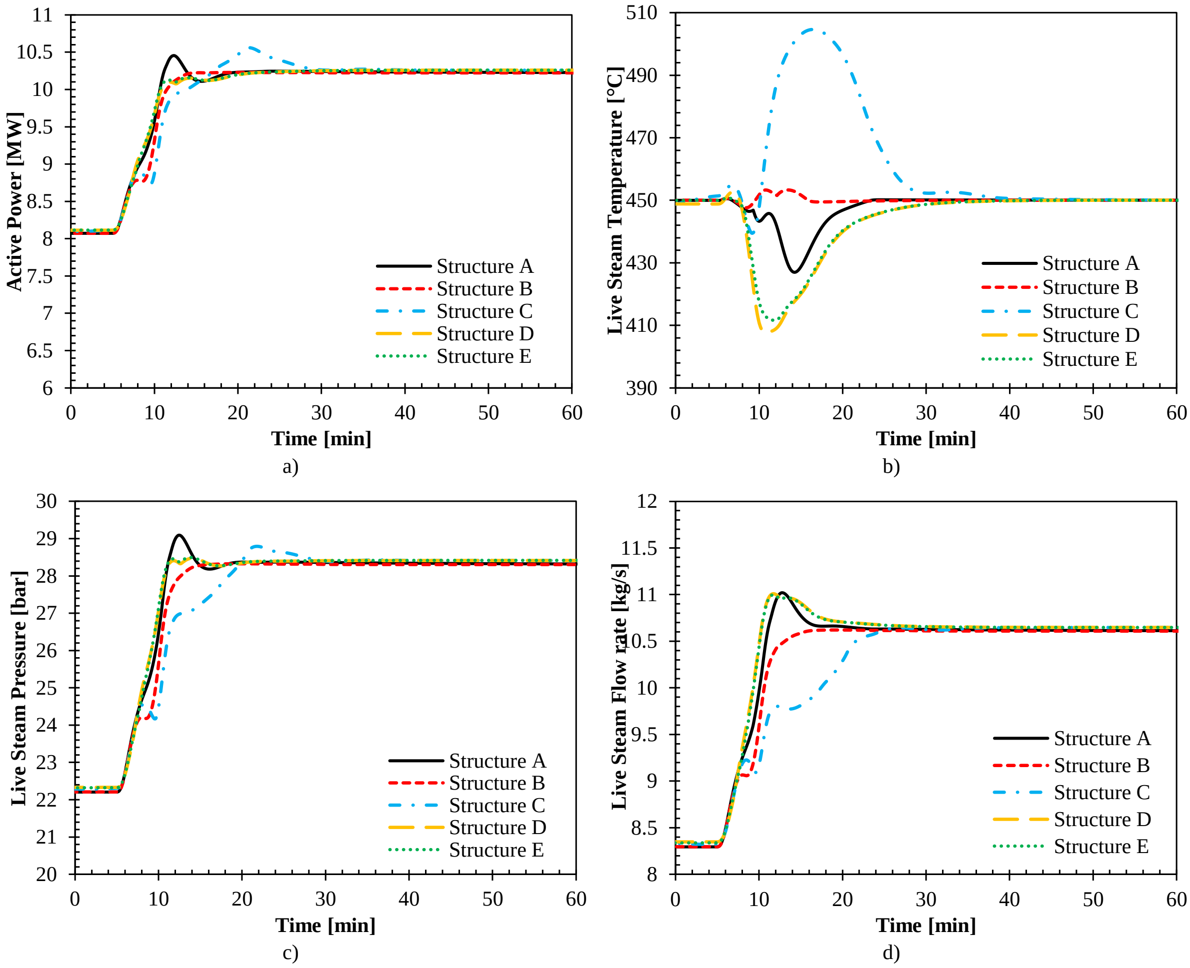

Figure 10: Transient response of the steam cycle to changes in GT load from 50% to 100% with a GT load change ramp rate of 10%/min, starting at time $t = 5$ min (Scenario 2). The response is presented for the five control structures defined in Section 2.3 for: a) steam turbine active power; b) live steam temperature; c) live steam pressure; and d) live steam flow rate.

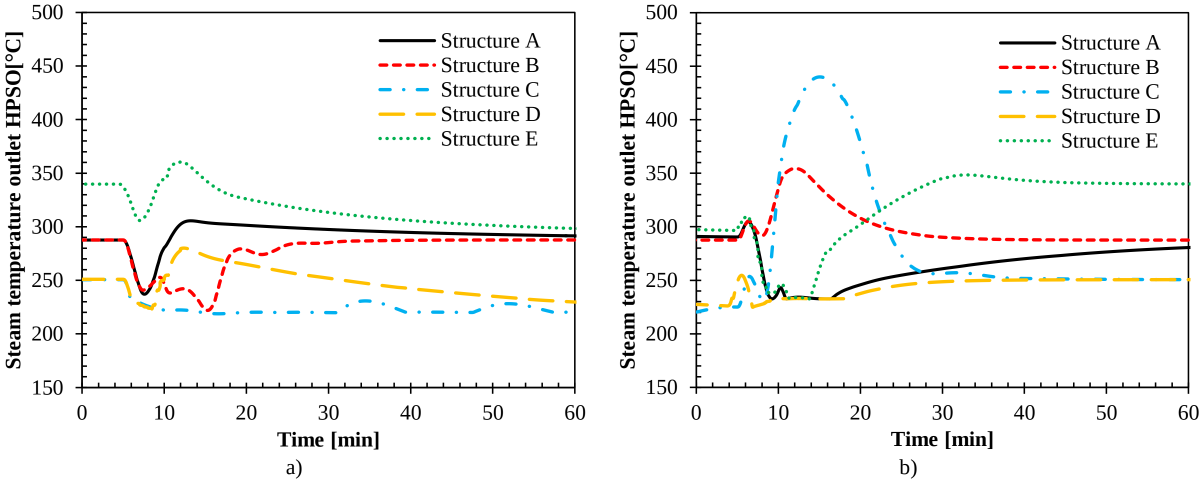

Figure 11: Transient response of the water/steam temperature at the outlet of the HPS0 recuperator for a) Scenario 1, and b) Scenario 2.

operating conditions than when feedback control is utilized in structure B, refer to Fig. 9. It can clearly be seen by the longer stabilization time required for the controlled variable $T_{HPSOs,out}$ in Fig. 11a. Control structure A with feedforward action in the feedwater mass flow rate controller brings the process towards stable conditions in less amount of time. This might be explained by the long feedback control loop in control structure B, which includes part of the thermal inertia of the OTSG in the loop, resulting in a slower response and oscillations. The feedforward action reduces the oscillations of feedwater mass flow rate sent to the OTSG, which results in more smooth transient steam turbine generator active power, transient live steam mass flow rate, and live steam temperature output trajectories. For control structures C, D, and E in which $T_{livesteam}$ was controlled, the results show that the control structure significantly influences the output trajectories of the steam cycle main process variables, including ST generator active power, and live steam temperature and pressure. This can be explained because the feedback controller includes the full thermal inertia of the OTSG in the control loop, making the response slower. Relatively large overshoots and oscillations in live steam temperature are observed for both control structures C and D. Slow oscillations around the final steady-state operating point are also observed in the feedwater mass flow rate when PI controller was utilized in control structure C, refer to Fig. 8a. This might necessitate attemperation control during fast load changes, if those overshoots in temperature are not allowed. When attemperation control was utilized via live steam attemperation, the overshoots during transient conditions in live steam temperature were avoided, as shown in control structure E in Fig. 9. In addition, a more smooth transient response was observed in the steam turbine generator active power. Note that for the control structures in which live steam attemperation was not utilized, the steady-state operating conditions at GT full load and 50% part load differ from the resulting ones with active attemperation (Fig. 8).

In Scenario 2 during loading, there is an increase of the heat transferred from the exhaust gas to the water/steam in the OTSG. More feedwater must be sent to balance the amount of steam being generated in the boiler. When comparing control structures A and B in which $T_{HPSOs,out}$ was controlled, a larger undershoot was found in live steam temperature when utilizing feedforward control (control structure A) on the feedwater mass flow rate control loop. This could be explained by the excess of steam being generated during transient conditions (overshoot in Fig. 10d). In this case, a more smooth transient response in steam turbine generator active power was found when utilizing feedback control with control structure B. For control structures in which the live steam temperature $T_{livesteam}$ was the controlled variable, i.e. control structures C, D, and E, the PI control without attemperation showed a very poor response (control structure C), resulting in long stabilization times with large overshoot in live steam temperature, see Fig. 10. The utilization of feedforward control (control structures D and E) resulted in a faster and more smooth transient response, see Fig. 10.

4. Conclusions

Model validation of a steam bottoming cycle at both design and off-design conditions with data from the Oseberg Field Center was performed with satisfactory results. These results show that the developed steady-state models for design and off-design simulations represent current technology performance of gas turbine based combined cycle with once-trough heat recovery steam generators. Therefore, the simulation results from the process models can be used as reference data for dynamic process model validation. The dynamic process model of the compact combined cycle was validated with steady-state and transient reference data. Steady-state validation results show the capability of the dynamic process model to capture the variability of steady-state operating conditions of the process for the whole operating window of the gas turbine (100% to 20% GT load). The implemented control structure brought the process to the correct operating conditions, showing the proper implementation of the regulatory control layer of the dynamic process model, including switching between sliding pressure and valve throttling control strategies. The validation results show that the dynamic process model can be utilized for transient performance analysis and control structure design. In addition, the validation with reference transient plant data showed the capability of the dynamic process model to capture the output trajectories of main process variables for load change transient events.

A case study on evaluation of transient performance of the process when applying different control structures and algorithms to the compact steam bottoming cycle was presented. This case study illustrates the potential of the model for its application in control structure design of the process early in the design stage of such power cycles. In addition, it shows the potential of physical modeling to provide better understanding of the interactions between control structures and the physical phenomena occurring in complex systems at plant system level. For common transient events in which the power plant load was changed driven by fast changes in GT load, applying feedforward control on the feedwater mass flow rate controller, that defines the water/steam flow network of the cycle, was required to avoid slow oscillations around the final steady-state operating conditions. If large overshoots in live steam temperature are to be avoided during the load change, attemperation might be required. The results presented in this work show the effectiveness of using steam attemperation with a spray of high pressure feedwater during fast load changes.

5. Acknowledgments

The authors acknowledge the partners ENGIE E&P Norge AS, Alfa Laval, Statoil, Marine Aluminium, SINTEF Energy Research, NTNU, and the Research Council of Norway, within the strategic Norwegian research program PETROMAKS2 (#233947), for their support.

Nomenclature

A_{heat}	heat transfer area (m^2)
d_{hyd}	hydraulic diameter (m)
F_{a}	tube arrangement factor (-)
h	specific enthalpy (J/kg)
K_{s}	Stodola's flow area coefficient
LHV	lower heating value (kJ/kg)
$\dot{m}$	mass flow rate (kg/s)
$\dot{m}_{LTE,rec}$	recirculated mass flow rate for feedwater temperature control (kg/s)
$\dot{m}_{steam}$	steam mass flow rate (kg/s)
Nu	Nusselt number
p	pressure (bar)
$p_{HPOTBout}$	boiler pressure (bar)
$p_{inletHRSGsteam}$	pressure (bar)
$p_{inletST}$	pressure (bar)
$p_{livesteam}$	pressure (bar)

Q heat transfer (W)

T temperature (°C)

$T_{HPEO,out}$ water temperature at oulet of economizer (°C)

$T_{HPSOs,out}$ steam temperature at oulet of boiling section (°C)

T_{fluid} temperature fluid (°C)

$T_{inletHRSGgas}$ temperature of exhaust gas at HRSG inlet (°C)

$T_{livesteam}$ live steam temperature (°C)

$T_{ouletHRSGgas}$ temperature of exhaust gas at HRSG outlet (°C)

T_{wall} temperature wall (°C)

t time (min)

t_r reference value from steady-state simulations in Thermoflow

t_s simulation result in Dymola

U overall heat transfer coefficient (W/m^{2}K)

V volume (m^3)

$\dot{W}_{ST}$ active power output (W)

$w_{dry,loss}$ dry steam turbine exhaust losses (kJ/kg)

$w_{st,loss}$ steam turbine exhaust losses (kJ/kg)

x vapor quality (-)

x_m mean step steam quality (-)

y moisture content (-)

α_g heat transfer coefficient gas side (W/m^{2}K)

α_s heat transfer coefficient steam side (W/m^{2}K)

β Baumann coefficient (-)

η_{dry} dry step efficiency (-)

η_{step}	corrected step efficiency (-)
λ	thermal conductivity (W/mK)
ρ	density (m^3)
FF	feed forward
GT	gas turbine
HP	high pressure
HP OTB	high pressure once-through boiler
HPE	high pressure economizer
HPS	high pressure superheater
HPSO OTB	superheater high pressure once-through boiler
HRSG	heat recovery steam generator
LP	low pressure section
LTE	low temperature economizer
ORC	organic Rankine cycle
OTSG	once-through heat recovery steam generator
PC	pressure controller
PI	proportional and integral feedback control
PID	proportional, integral, derivative
PT	pressure transmitter
RE	relative error
ST	steam turbine
TC	temperature controller
TPL	thermal power library
TT	temperature transmitter
WHRU	waste heat recovery unit

References

[1] T.-V. Nguyen, L. Tock, P. Breuhaus, F. Maréchal, B. Elmegaard, Oil and gas platforms with steam bottoming cycles: System integration and thermoenvironomic evaluation, Applied Energy 131 (2014) 222–237.

[2] L. Pierobon, A. Benato, E. Scolari, F. Haglind, S. A., Waste heat recovery technologies for offshore platforms, Applied Energy 136 (2014) 228–241.

[3] H. T. Walnum, P. Nekså, L. O. Nord, T. Andresen, Modelling and simulation of CO2 (carbon dioxide) bottoming cycles for offshore oil and gas installations at design and off-design conditions, Energy 59 (2013) 513–520.

[4] L. Riboldi, L. O. Nord, Concepts for lifetime efficient supply of power and heat to offshore installations in the North Sea, Energy Conversion and Management 148 (2017) 860–875.

[5] L. O. Nord, E. Martelli, O. Bolland, Weight and power optimization of steam bottoming cycle for offshore oil and gas installations, Energy 76 (2014) 891–898.

[6] L. O. Nord, O. Bolland, Steam bottoming cycles offshore—Challenges and possibilities, Journal of Power Technology 92 (3) (2012) 201–207.

[7] L. O. Nord, O. Bolland, Design and off-design simulations of combined cycles for offshore oil and gas installations, Applied Thermal Engineering 54 (1) (2013) 85–91.

[8] J. Bimüller, L. O. Nord, Process simulation and plant layout of a combined cycle gas turbine for offshore oil and gas installations, Journal of Power Technologies 95 (1) (2015) 40–47.

[9] L. Riboldi, L. O. Nord, Lifetime assessment of combined cycles for cogeneration of power and heat in offshore oil and gas installations, Energies 10 (6) (2017) 744.

[10] L. Pierobon, E. Casati, F. Casella, F. Haglind, P. Colonna, Design methodology for flexible energy conversion systems accounting for dynamic performance, Energy 68 (2014) 667–679.

[11] A. Benato, L. Pierobon, F. Haglind, A. Stoppato, Dynamic performance of a combined gas turbine and air bottoming cycle plant for off-shore applications, ASME 2014 12th Biennial Conference on Engineering Systems Design and Analysis, ESDA 2014 2.

[12] M. F. Brady, Design aspects of once through systems for heat recovery steam generators for base load and cyclic operation, Materials at High Temperatures 18 (4) (2001) 223–229.

[13] P. Colonna, H. van Putten, Dynamic modeling of steam power cycles: Part IModeling paradigm and validation, Applied Thermal Engineering 27 (2) (2007) 467 – 48.

[14] F. Alobaid, R. Starkloff, S. Pfeiffer, K. Karner, B. Epple, H.-G. Kim, A comparative study of different dynamic process simulation codes for combined cycle power plants Part A: Part loads and off-design operation, Fuel 153 (2015) 692 – 706.

[15] F. Alobaid, R. Starkloff, S. Pfeiffer, K. Karner, B. Epple, H.-G. Kim, A comparative study of different dynamic process simulation codes for combined cycle power plants Part B: Start-up procedure, Fuel 153 (2015) 707 – 716.

[16] H. van Putten, P. Colonna, Dynamic modeling of steam power cycles: Part II Simulation of a small simple Rankine cycle system, Applied Thermal Engineering 27 (14) (2007) 2566 – 2582.

[17] M. Valdés, J. L. Rapún, Optimization of heat recovery steam generators for combined cycle gas turbine power plants, Applied Thermal Engineering 21 (11) (2001) 1149 – 1159.

[18] C. Celis, G. R. Pinto, T. Teixeira, rica Xavier, A steam turbine dynamic model for full scope power plant simulators, Applied Thermal Engineering 120 (2017) 593 – 602.

[19] N. Mertens, F. Alobaid, T. Lanz, B. Epple, H.-G. Kim, Dynamic simulation of a triple-pressure combined-cycle plant: Hot start-up and shutdown, Fuel 167 (2016) 135 – 148.

[20] Thermoflow Version 25, Thermoflow Inc., 2015.

[21] www.modelica.org, Modelica Association, 2016.

[22] A. Benato, A. Stoppato, A. Mirandola, Dynamic behavior analysis of a three pressure level heat recovery steam generator during transient operation, Energy 90 (2015) 1595–1605.

[23] K. Wellner, T. Marx-Schubach, G. Schmitz, On the dynamic behaviour of coal fired power plants with post-combustion CO2 capture, Industrial and Engineering Chemistry Research 55 (46) (2016) 12038–12045.

[24] R. M. Montañés, S. O. Gardarsdóttir, F. Normann, F. Johnsson, L. O. Nord, Demonstrating load-change transient performance of a commercial-scale natural gas combined cycle power plant with post-combustion CO2 capture, International Journal of Greenhouse Gas Control 63 (2017) 158–174.

[25] R. M. Montañés, J. Windahl, J. Pålsson, M. Thern, Dynamic modeling of a parabolic trough solar thermal power plant with thermal storage using Modelica, Heat Transfer Engineering 39 (3) (2018) 277–292.

[26] W. Wagner, J. R. Cooper, A. Dittmann, J. Kijima, H. J. Kretzschmar, A. Kruse, R. Mareš, K. Oguchi, H. Sato, I. Stöcker, O. Šifner, Y. Takaishi, I. Tanishita, J. Trübenbach, T. Willkommen, The IAPWS industrial formulation 1997 for the thermodynamic properties of water and steam, Journal of Engineering for Gas Turbines and Power 122 (1) (2000) 150–180.

[27] ESCOA Fintube Manual, ESCOA Corp., Tulsa, OK, USA, 1979.

[28] R. C. Spencer, K. C. Cotton, C. N. Cannon, A method for predicting the performance of steam turbine generators 16,500 kW and larger, Journal of Engineering for Power 85 (4) (1963) 249–298.

[29] Dymola, Dassault Systemes, 2016.

[30] Thermal Power Library, Modelon AB, 2016.

[31] P. J. Dechamps, Modelling the transient behavior of combined cycle plants, ASME International Gas Turbine and Aero-engine Congress and Exposition 4 (1) (1994) pp. 8.

[32] VDI-Värmeatlas, 9th edition, Springer, 1997.

[33] M. Dumont, G. Heyen, Mathematical modelling and design of an advanced once-through heat recovery steam generator, Computers and Chemical engineering 28 (2004) 651–660.

[34] T. Hoppe, F. Gottelt, S. Wischhusen, Extended modelica model for heat transfer of two-phase flows in pipes considering various flow patterns, Proceedings of the 12th International Modelica Conference, Prague, Czech Republic (2017) 467–476.

[35] F. Alobaid, N. Mertens, R. Starkloff, T. Lanz, C. Heinze, B. Epple, Progress in dynamic simulation of thermal power plants, Progress in Energy and Combustion Science 59 (2017) 79–162.

[36] K. Jordal, P. A. M. Ystad, R. Anantharaman, A. Chikukwa, O. Bolland, Design-point and part-load considerations for natural gas combined cycle plants with post combustion capture, International Journal of Greenhouse Gas Control 11 (2012) 271–282.